Inorg. Chem. **2009**, *48*, 4003−4009

Nearly Monodisperse $CuInS_2$ Hierarchical Microarchitectures for Photocatalytic H_2 Evolution under Visible Light

Lei Zheng, Yang Xu, Yan Song, Changzheng Wu, Miao Zhang, and Yi Xie*

Department of Nanomaterials and Nanochemistry, Hefei National Laboratory for Physical Sciences at Microscale, University of Science and Technology of China, Hefei, Anhui 230026, P. R. China

Received September 4, 2008

An enhanced visible-light-driven photocatalyst, $CuInS_2$, was prepared by a facile in situ formed template solvothermal route. The products show complex hierarchical architectures assembled from interleaving two-dimensional microcrystals and near monodispersity. It is interesting to see revealed a phase conversion process from binary sulfide to ternary sulfide as well as morphology evolution, investigated by X-ray diffraction and scanning electron microscopy. The involved CuS hierarchitectures form in situ and then act as the self-sacrificed templates, resulting in the obtained $CuInS_2$ inheriting the hierarchical architectures and monodispersity. More importantly, a much higher average hydrogen yield of 59.4 μmol/h for 1.0 g of photocatalyst under visible light irradiation than in the previously reported results has been attained over the obtained $CuInS_2$ hierarchitectures loaded with cocatalyst Pt, which may be due to the benefits inheriting from CuS templates such as monodispersity, high surface area, and permeability for providing sufficient visible light response and more reaction sites for photocatalysis in aqueous solution.

1. Introduction

The concern over limited global energy and environmental degradation has led to increasing efforts directed toward the utilization of solar energy, which can supply a huge amount of energy on the earth's surface that far exceeds all human energy needs.[1] Solar water heaters and photovoltaic and electrochemical solar cells that convert solar energy into heat or electricity have also been deeply investigated for improving energy conversion efficiency.[2−4] However these techniques still have their own limitations in terms of energy density, energy storage, cost, diversity, and instability in direct conversion.[5] In a process that is similar to photosynthesis, solar energy can also be used for photocatalytic splitting of water for H_2 evolution with a conversion of solar energy to chemical energy and for energy storage.[1,6] Hydrogen fuel is a potentially clean and renewable source with many advantages, such as high energy density and convenience for storage and transport.[7] Thus, development of semiconductor photocatalysts fitting for H_2 evolution under solar illumination has received a great deal of attention. However, many reported photocatalysts[8−11] with wide band gaps (3 eV or above) take UV light as the light source for photocatalytic H_2 evolution and do not absorb visible light, which composes the major part of the solar spectrum. Thus, developing highly active photocatalysts with a visible light response is still an important theme in the current photocatalysis field.

In recent years, the ternary sulfide semiconductors, such as $ZnInS_2$[12] and $AgIn_5S_8$,[13] have been receiving considerable research interest due to their potential photocatalytic activity for H_2 evolution under visible light irradiation. But another important ternary sulfide, $CuInS_2$, used as a photocatalyst for hydrogen evolution from aqueous sulfite solution was

* To whom correspondence should be addressed. Fax: 86-551-3606266. E-mail: yxie@ustc.edu.cn.

(1) Frank, E.; Osterloh, E. *Chem. Mater.* **2008**, *20*, 35.
(2) Huynh, W. U.; Dittmer, J. J.; Alivisatos, A. P. *Science* **2002**, *295*, 2425.
(3) Bach, U.; Lupo, D.; Comte, P.; Moser, J. E.; Weissortel, F.; Salbeck, J.; Spreitzer, H.; Gratzel, M. *Nature (London)* **1998**, *395*, 583.
(4) Gratzel, M. *Nature (London)* **2001**, *414*, 338.
(5) Law, M.; Greene, L. E.; Johnson, J. C.; Saykally, R.; Yang, P. D. *Nat. Mater.* **2005**, *4*, 455.
(6) Fujishima, A.; Honda, K. *Nature (London)* **1972**, *238*, 37.
(7) Turner, J. A. *Science* **2004**, *305*, 972.
(8) Kudo, A.; Omori, K.; Kato, H. *J. Am. Chem. Soc.* **1999**, *121*, 11459.
(9) Reber, J. F.; Meier, K. *J. Phys. Chem.* **1984**, *88*, 5903.
(10) Sato, J.; Saito, N.; Yamada, Y.; Maeda, K.; Takata, T.; Kondo, J. N.; Hara, M. H.; Kobayashi, K.; Domen, K. *J. Am. Chem. Soc.* **2005**, *127*, 150.
(11) Kato, H.; Asakura, K.; Kudo, A. *J. Am. Chem. Soc.* **2003**, *125*, 3082.
(12) Lei, Z.; You, W.; Liu, M.; Zhou, G.; Takata, T.; Hara, M.; Domen, K.; Li, C. *Chem. Commun.* **2003**, *17*, 2142.
(13) Chen, D.; Ye, J. *J. Phys. Chem. Solids* **2007**, *68*, 2317.

10.1021/ic802399f CCC: $40.75
Published on Web 04/02/2009

just investigated under UV light irradiation,[14] and the amount of H_2 evolution is rather low, even with Ag_2S as a cocatalyst. The band gap of $CuInS_2$ (Eg $\sim$ 1.53 eV) is well-matched to the AM0 solar spectrum with a high absorption coefficient for photovoltaic performance.[15] For example, three-dimensional (3-D) $TiO_2/CuInS_2$ nanocomposite solar cells[16] have been fabricated with a remarkable energy conversion efficiency of 5%, which gives us hope that $CuInS_2$ is a promising material with a visible-light response and might be a good candidate for visible-light-driven photocatalytic H_2 evolution from water.

In order to obtain excellent photocatalytic activity, the combination of materials-related characteristics has been investigated, including crystallinity, monodispersity, surface area, and permeability, which provide sufficient visible-light response and more reaction sites, a short bulk-to-surface diffusion distance for e^- and h^+, and monodisperse cocatalyst nanostructures, which contribute to an efficient charge separation, a fast transport of the photogenerated carriers, and a fast photochemical reaction at the photocatalyst/electrolyte interface.[17−20] Therefore, by improving the dispersity, crystallinity, and surface area, we could further improve the photocatalytic activity of the pure $CuInS_2$ photocatalyst, especially toward the visible-light response goal.

The conventional synthesis routes of ternary sulfides such as spray pyrolysis[21] and chemical vapor deposition[24] need either a high temperature (above 400 °C) or special devices,[21−26] and the previously reported hydrothermal[27] or solvothermal[28] techniques brought on products with several disadvantages, such as particle agglomeration, noncrystallinity, poor dispersity, and so forth, which go against their photocatalysts' ability. Developing a route to prepare photocatalysts with monodispersity and a hierarchical architecture assembled by nanoscaled building blocks may furnish us with a promising way for improving photocatalytic activity.[29,30] The rough surfaces of the hierarchical architectures with increased area and permeability could provide ideal activity sites for photocatalytic reactions.[31] However, previous research has indicated that the direct fabrication of ternary sulfide hierarchitectures is more complicated than that of binary sulfides. Meanwhile, the binary sulfides such as CuS with different morphologies have been easily and controllably synthesized.[32−34] Therefore, the in situ formed binary sulfide template route may provide a convenient and effective approach for constructing ternary sulfide hierarchical architectures.

In this study, we report a simple, one-pot route for large-scale preparation of nearly monodisperse $CuInS_2$ with hierarchical architectures using in situ formed CuS template in high-boiling point solvent of triethylene glycol. The phase and morphology evolution processes from the intermediate CuS template to the final $CuInS_2$ product were investigated detailedly, and verified to be a new efficient and controllable route to ternary sulfide hierarchitectures. More importantly, the obtained $CuInS_2$, as a photocatalyst, exhibits remarkable photocatalytic activity for H_2 evolution from water than previously reported in the presence of Na_2S/Na_2SO_3 as sacrificial electron donors under visible light irradiation.

2. Experimental Section

All chemical reagents in this work were purchased from the Shanghai Chemical Company. They were of analytical grade and used without further purification.

Synthesis of Hierarchical $CuInS_2$ Microarchitectures. In a typical synthesis, 1.0 mmol CuCl, 1.0 mmol $InCl_3 \cdot 4H_2O$, and 2.5 mmol sublimed sulfur powders were dispersed in 30 mL of triethylene glycol under vigorous stirring, and then ultrasonication for 20 min to form an opaque yellow-green suspension. Afterward, the suspension was transferred into a 40 mL Teflon-lined stainless steel autoclave. The autoclave was sealed and maintained at 200 °C for 48 h. After cooling to room temperature naturally, the final dark products were collected by centrifuging the mixture, washed with absolute ethanol and distilled water several times, and then dried under a vacuum at 60 °C overnight for further characterization.

Sample Characterization. The samples were characterized by X-ray powder diffraction (XRD) with a Japan Rigaku Dmax X-ray diffractometer equipped with graphite monochromatized high-intensity Cu Kα radiation (λ = 1.54178Å). The transmission electron microscopy (TEM) images were obtained using a Hitachi Model H-800 instrument with a tungsten filament, using an accelerating voltage of 200 kV. High-resolution transmission electron microscopy (HRTEM) images and electron diffraction (ED) patterns were carried out on a JEOL-2010 transmission electron microscope at an acceleration voltage of 200 kV. The field emission scanning electron microscopy (FESEM) images were taken on a FEI Sirion-200 scanning electron microscope. UV−vis spectra were recorded on a Solid Spec-3700 spectrophotometer at room temperature.

Photocatalytic Test. Photocatalytic hydrogen evolution was carried out in a closed gas circulation and evacuation system equipped with a top-irradiation Pyrex cell reactor connected to a water bath. The temperature of the reactant solution was maintained

(14) Kobayakawa, K.; Teranishi, A.; Tsurumaki, T.; Sato, Y.; Fujishima, A. *Electrochim. Acta* **1992**, *37*, 465.
(15) Stephanie, L.; Castro, S. G.; Bailey, R. P.; Raffaelle, K.; Banger, K.; Aloysius, F. H. *Chem. Mater.* **2003**, *15*, 3142.
(16) Nanu, M.; Schoonman, J.; Goossens, A. *Nano Lett.* **2005**, *5*, 1716.
(17) Bao, N.; Shen, L.; Takata, T.; Domen, K. *Chem. Mater.* **2008**, *20*, 110.
(18) Kudo, A.; Kato, H.; Tsuji, I. *Chem. Lett.* **2004**, *33*, 1534.
(19) Fox, M. A.; Dulay, M. T. *Chem. Rev.* **1993**, *83*, 341.
(20) Bao, N.; Shen, L.; Takata, T.; Domen, K.; Gupta, A.; Yanagisawa, K.; Grimes, A. C. *J. Phys. Chem. C* **2007**, *111*, 17527.
(21) Isomura, T.; Kariya, T.; Shirakata, S. *Cryst. Res. Technol.* **1996**, *31*, 523.
(22) Yamamoto, Y.; Yamaguchi, Y.; Denizu, Y.; Tanaka, T.; Yoshida, A. *Thin Solid Films* **1996**, *282*, 372.
(23) Stolt, L.; Hedstrom, J.; Kessler, J.; Ruckh, M.; Velthaus, K.; Schock, H. W. *Appl. Phys. Lett.* **1993**, *62*, 597.
(24) Nomura, R.; Sekl, Y.; Matsuda, H. *J. Mater. Chem.* **1992**, *2*, 765.
(25) Das, K.; Datta, A.; Chaudhuri, S. *Cryst. Growth. Des.* **2007**, *8*, 1547.
(26) Xiao, J.; Xie, Y.; Tang, R.; Qian, Y. *J. Solid State Chem.* **2001**, *161*, 179.
(27) Jiang, Y.; Wu, Y.; Mo, X.; Yu, W.; Xie, Y.; Qian, Y. *Inorg. Chem.* **2000**, *39*, 2964.
(28) Jiang, Y.; Wu, Y.; Yuan, S.; Xie, B.; Zhang, S.; Qian, Y. *J. Mater. Res.* **2001**, *16*, 2805.
(29) Lu, Q.; Gao, F.; Komarneni, S. *J. Am. Chem. Soc.* **2004**, *126*, 54.
(30) Ding, Y.; Shen, X.; Gomez, S.; Luo, H.; Aindow, M.; Steven, L. *Adv. Funct. Mater.* **2006**, *16*, 549.
(31) Zhao, Q.; Xie, Y.; Zhang, Z.; Bai, X. *Cryst. Growth. Des.* **2007**, *7*, 153.
(32) Wu, C.; Yu, S.; Markus, A. *Chem. Mater.* **2006**, *18*, 3599.
(33) Yao, Z.; Zhu, X.; Wu, C. *Cryst. Growth. Des.* **2007**, *7*, 1256.
(34) Li, B.; Xie, Y.; Xue, Y. *J. Phys. Chem. C* **2007**, *111*, 12181.

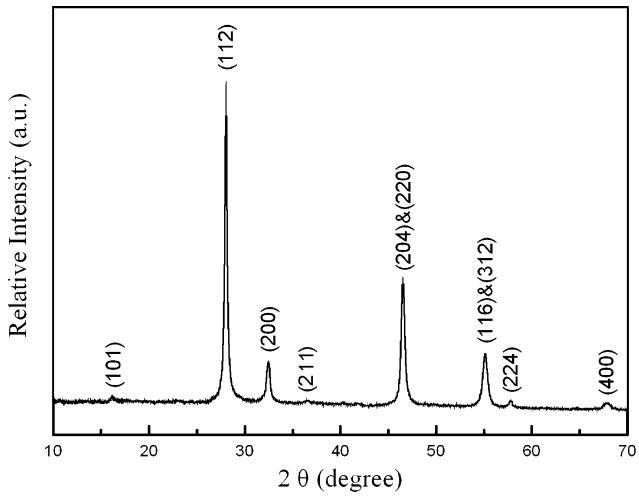

Figure 1. XRD pattern of as-prepared $CuInS_2$ product.

at room temperature by providing a flow of cooling water during the photocatalytic reaction. Prior to the photocatalytic reaction, Pt co-photocatalyst was loaded on $CuInS_2$ powders in situ through a 0.5 h photoreduction of a 0.5 wt % H_2PtCl_6 solution with UV light irradiation using a 450 W high-pressure Hg lamp. Approximately 0.250 g of Pt-loaded $CuInS_2$ photocatalyst was dispersed by a magnetic stirrer in 200 mL of aqueous solution containing 0.35 M Na_2SO_3 and 0.25 M Na_2S as sacrificial reagents. The photocatalysts were irradiated with visible light ($\lambda \geq 420$nm) using a cutoff filter from a 500 W Xe lamp. The amount of hydrogen evolved was determined with gas chromatography (Shimadzu GC-14C, argon carrier) every hour.

3. Results and Discussion

Synthetic Route and Characterization of Hierarchical $CuInS_2$ Architectures. Hierarchical $CuInS_2$ architectures were obtained by the reaction between CuCl and $InCl_3$ and S powders dispersed in a triethylene glycol solvent. The phase and crystallinity of the $CuInS_2$ product were well-characterized using XRD techniques. As shown in Figure 1, all of the diffraction peaks match well with the standard data of chalcopyrite-type $CuInS_2$ with tetragonal lattice parameters of $a = 5.522$ Å and $c = 11.13$ Å (JCPDS card No. 85-1575; I-42D). The XRD pattern shows that the product is devoid of any detectable impurities such as CuS or In_2S_3, indicating that the obtained products consist of pure chalcopyrite-type $CuInS_2$.

The morphology of the $CuInS_2$ hierarchitectures was examined by scanning electron microscopy (SEM) and TEM. The typical SEM image, as shown in Figure 2A and B, gives a panoramic picture of the product, revealing that the product consists almost entirely of nearly monodisperse spherical hierarchitectures (100% morphological yield) with an average diameter of 5.0 μm. Figure 2C shows the high-magnification FESEM image of a single $CuInS_2$ hierarchical microsphere, which is in fact built by many interleaving two-dimensional flakes with a thickness of about 15∼20 nm in a perfectly aligned manner. From the TEM image shown in Figure 2D, it can be observed that the flakes align with one another to form a sphere, and all of the spheres have a uniform morphology. Figure 2E and F show the HRTEM image and the selected area electron diffraction (SAED) pattern of a portion of the flakes ultrasonically exfoliated from a microsphere. The SAED pattern shows that the flakes are single crystals with a tetragonal lattice corresponding to chalcopyrite-type $CuInS_2$. The suitably crystalline nature is also revealed by the lattice fringes of 0.32 nm, assigned to the (112) crystal planes. The energy-dispersive spectra (EDS) analysis of the flakes shown in Figure 2G demonstrates that the chemical components only consisted of Cu, In, and S, and their molar ratio is 28:27:45 (the signals of Mo and C are from the molybdenum grid), in agreement with the above XRD results.

Phase Conversion and Morphology Evolution of Hierarchical $CuInS_2$ Architectures. To understand the formation mechanism of the $CuInS_2$ hierarchitectures, time-dependent crystal morphology evolution through interception of the intermediate products was performed at different stages of 0.5, 1, 3, 12, 24, and 36 h. In the solvothermal process, the reaction time plays an important role in determining the phase conversion of the products. The integration of electron microscopy images and the corresponding XRD patterns of the different intermediate samples clearly reveal the growth process, as shown in Figure 3. At the initial stage (0.5 h), the primary products were the irregular spherical architectures comprised of small nanoparticles (Figure 3A), and the XRD pattern was apparently composed of peaks corresponding to sulfur and CuS (Figure 3a). When the reaction time increased to 1 h, all of these products became uniform monodisperse microspheres with an average diameter of about 1.5 μm, as shown in Figure 3B. The inset of the high-magnification SEM image reveals that these microspheres are built of closely packed small flakes. All detectable peaks in the relevant XRD pattern (Figure 3b) could readily be indexed to hexagonal covellite-phase CuS (JCPDS card no. 06-0464). When the reaction time is prolonged to 3 h, the minor tetragonal $CuInS_2$ crystalline phase appears with the existence of the main CuS phase, as indicated in the XRD pattern (Figure 3c). From the corresponding SEM image (Figure 3C), on the peeled area of spheres, it could be observed that the small flakes tend to aggregate together and form large flakes on the periphery, and as a result, these microarchitectures looked like larger spheres in shape. As the reaction proceeded to 12 h, the obtained products grew to microspheres constructed by loosely packed flakes with an average diameter of 3.5−4.0 μm. Both hexagonal CuS and tetragonal $CuInS_2$ phases could be found in the XRD pattern (Figure 3d), but the XRD pattern evidently indicates that all diffraction peaks of $CuInS_2$ became stronger while the diffraction peak intensities of CuS decreased. At a reaction time of 24 h, the obtained intermediate samples, as shown in Figure 3E, were composed of many relatively homogeneous hierarchitectures with slightly increased size. XRD patterns, as shown in Figure 3e, also indicate that the proportion of $CuInS_2$ is rather high up to that point. After an elongated reaction for 36 h, the uniform morphology of nearly monodisperse microspheres could be obtained, as shown in Figure 3F. The size of microspheres built with larger interleaving flakes increased to about 5.0 μm. The

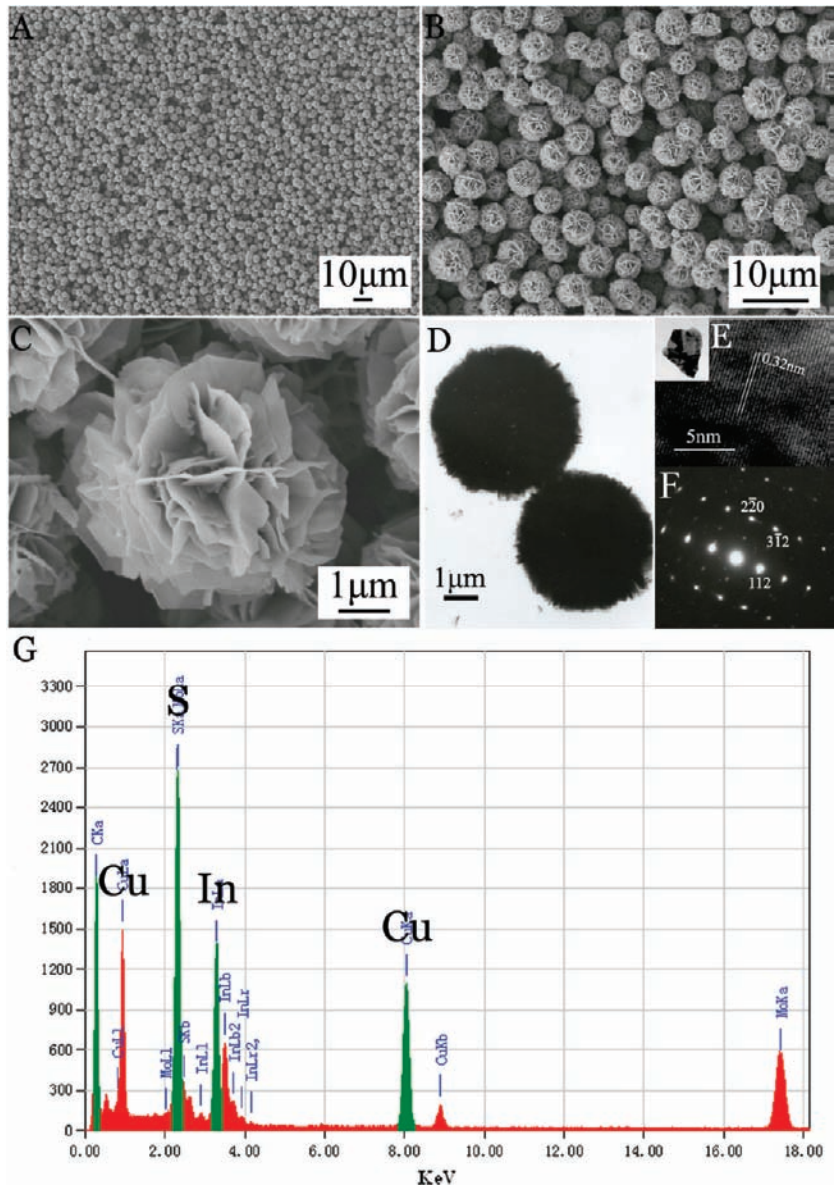

Figure 2. Representative SEM and TEM images of $CuInS_2$ hierarchitectures: (A and B) low-magnification FESEM images, (C) high-magnification SEM image, (D) TEM image, (E) HRTEM image, (F) the corresponding ED pattern, and (G) EDS spectrum.

XRD investigation shown in Figure 3f indicates that the sample is almost pure $CuInS_2$ with a hardly detectable CuS phase, and the crystallinity of the products indeed increased. Hence, an evolution of tetragonal $CuInS_2$ hierarchitectures from the in situ formed hexagonal CuS hierarchitectures as self-sacrificed templates was clearly demonstrated by the combined XRD patterns and microscopic images.

On the basis of the above experimental evidence, we proposed a reasonable mechanism for the formation of $CuInS_2$ hierarchitectures, as described in Scheme 1. The initial step is the formation of nearly monodisperse CuS templates with controllable morphology. Under these solvothermal conditions, the sulfur powders play a dual role, not only as the reagent but also as the original liquid-droplet template for fabricating CuS microspheres,[35] which will warrant well the monodispersity and homogeneous morphology for the final products. In the high-boiling point and viscous solvent of triethylene glycol, the added solid-state sulfur powders could be finely dispersed and suspended under vigorous stirring and ultrasonication. During the heating process of solvothermal reaction, sulfur powders could transform to spherical sulfur liquid droplets due to the surface tension at the temperature above its melting point (120 °C at normal atmosphere). Since elemental sulfur could easily oxidize Cu^I to form binary sulfide CuS,[35] other reactions to ternary sulfide or binary sulfide In_2S_3 are relatively inhibited. Simultaneously, the resulted CuS shell outside the melted sulfur droplets may act as an inhibitor and prevent the liquid droplets from further aggregating, resulting in the intermediates obtained after 0.5 h of heating followed by fast cooling being monodisperse microspheres (Figure 3A). The in situ formed CuS shell has been confirmed by its XRD pattern, as shown in Figure 3a. With the prolonged reaction, CuS nanoparticles grow into small flakes, exhibiting the growth

(35) Wan, S.; Guo, F.; Shi, L.; Peng, Y.; Liu, X.; Zhang, Y.; Qian, Y. *J. Mater. Chem.* **2004**, *14*, 2489.

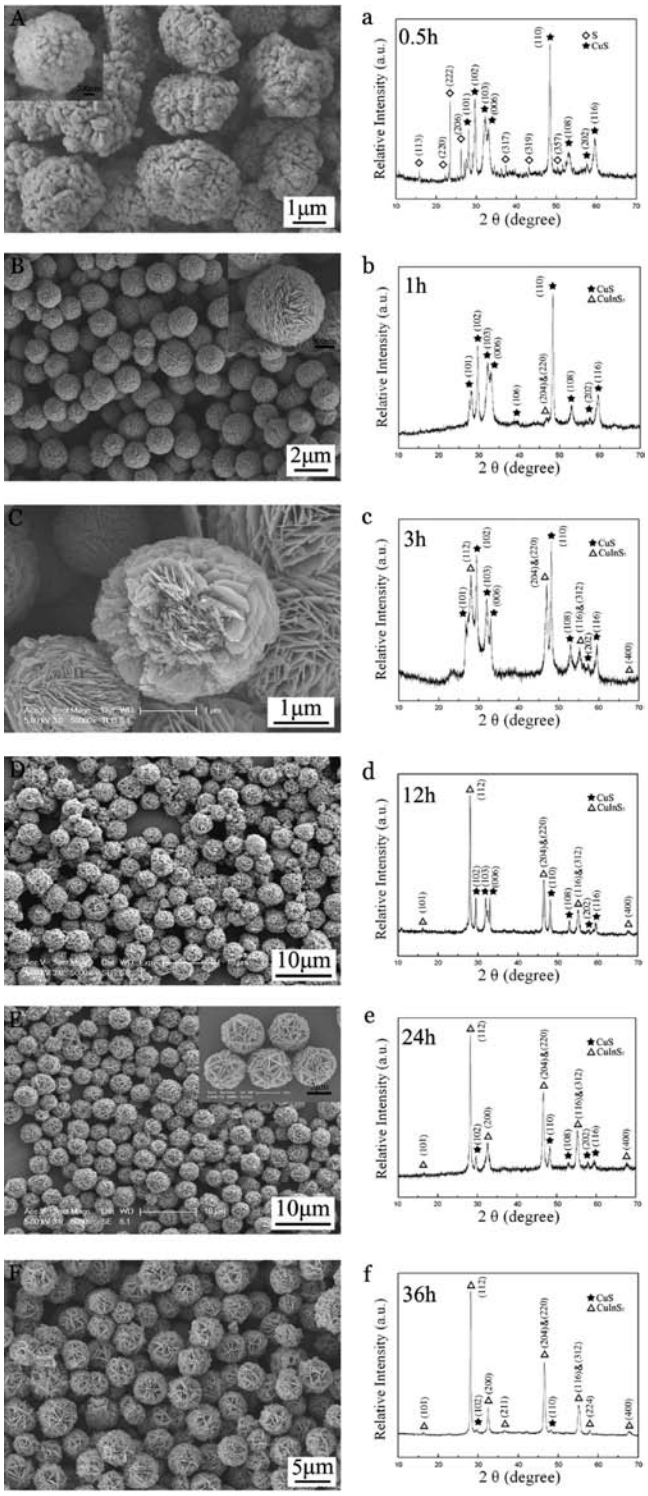

Figure 3. SEM images and XRD patterns (in which S, CuS, and $CuInS_2$ are symbolized by diamonds, stars, and triangles, respectively) of intermediate products prepared with CuCl, $InCl_3 \cdot 4H_2O$, and S at 200 °C for different reaction times. Electron microscopy images: (A) 0.5 h, (B) 1 h, (C) 3 h, (D) 12 h, (E) 24 h, (F) 36 h. XRD patterns: (a) 0.5 h, (b) 1 h, (c) 3 h;, (d) 12 h, (e) 24 h, (f) 36 h.

characteristic habit for hexagonal CuS,[36−38] and as a result, hierarchical microspheres consisting of irregular flakes as building blocks could be obtained. Then, the in situ formed CuS hierarchical microspheres serving as the self-sacrificed templates react with the remaining $InCl_3$ and Cu^{II} and are reduced to Cu^{I} by triethylene glycol to form $CuInS_2$ continuously, which still retains the morphology of the binary sulfide. In this process, as the CuS templates are consumed, the small $CuInS_2$ flakes form on the CuS/solution interface gradually. Similarly, newly formed $CuInS_2$ flakes become larger in size and the crystallinity of the products is indeed gradually increased, due to the Ostwald ripening growth process. Finally, the large flakes perfectly align from the center to the surface and knit to form hierarchical architectures.

To further understand the influences on controlling the morphology of $CuInS_2$ from CuS hierarchitectures, we investigate the solvothermal reaction of CuCl and sulfur in triethylene glycol. The CuS hierarchitectures can be easily prepared via a solvothermal process, and the time-dependent experiments further reveal that the binary sulfide CuS hierarchitectures also take a similar morphology evolution process to that of ternary sulfide $CuInS_2$ (see Figure S1 in the Supporting Information), from microspheres built by closely packed flakes to the uniform microcrystalline hierarchitectures, which maybe evidence that the obtained $CuInS_2$ hierarchitectures were directly transformed from the covellite CuS and thus inherited the hierarchical morphology.

It is known that the hexagonal type of covellite CuS posesses a highly anisotropic crystal structure that consists of alternating $CuS_4-CuS_3-CuS_4$ layers and S−S layers stacking along the *c* axis,[38] whereas the chalcopyrite-type $CuInS_2$ crystal contains equivalent sites for Cu and In atoms which are coordinated by four S atoms to form a CuS_4 (or InS_4) tetrahedron (Figure 4). The structure similarities of CuS and $CuInS_2$ give some hints toward the explanation of the phase conversion in situ and $CuInS_2$ inheriting the hierarchical microarchitectures. A further solvothermal process of the preobtained CuS hierarchitectures with $InCl_3 \cdot 4H_2O$ in triethylene glycol gives the $CuInS_2$ hierarchitectures with well-inherited morphology (see Figure S3 in the Supporting Information), confirming the template role of CuS microarchitectures.

Photocatalytic Activity of As-Obtained $CuInS_2$ Hierarchitectures. The optical absorption properties of a semiconductor, which are relevant to the electronic structure features, are recognized as key factors in determining its photocatalytic activity.[39] Figure 5 shows the optical properties of as-prepared $CuInS_2$ microarchitectures characterized by UV−vis absorption spectra, indicating that hierarchical microspheres of $CuInS_2$ display photo absorption properties mainly in the visible light region and have a broad absorption peak at around 620 nm, which exhibits a blue-shift phenomenon on comparison with the absorption peak value of previously reported results[26] and the bulk $CuInS_2$ (at 810 nm). The band gap energies can be estimated by a related curve of $(\alpha h\nu)^2$ versus photon energy (α = absorbance, h = Planck's constant, and ν = frequency) plotted in the inset

(36) Cordova, R.; Gomez, H.; Schrebler, R.; Cury, P.; Orellana, M.; Grez, P.; Leinen, D.; Ramos-Banrado, J. R.; Rio, D. R. *Langmuir* **2002**, *18*, 8647.
(37) Wang, X.; Xu, C.; Zhang, Z. *Mater. Lett.* **2006**, *60*, 345.
(38) Wang, K.; Li, G.; Li, J. *Cryst. Growth. Des.* **2007**, *7*, 2265.
(39) Zhou, L.; Wang, W. Z.; Liu, S. W. *J. Mol. Catal. A: Chem.* **2006**, *252*, 120.

Scheme 1. Schematic Description of Morphology Evolution (I) and the Proposed Formation Mechanism (II) of the $CuInS_2$ Hierarchitectures[a]

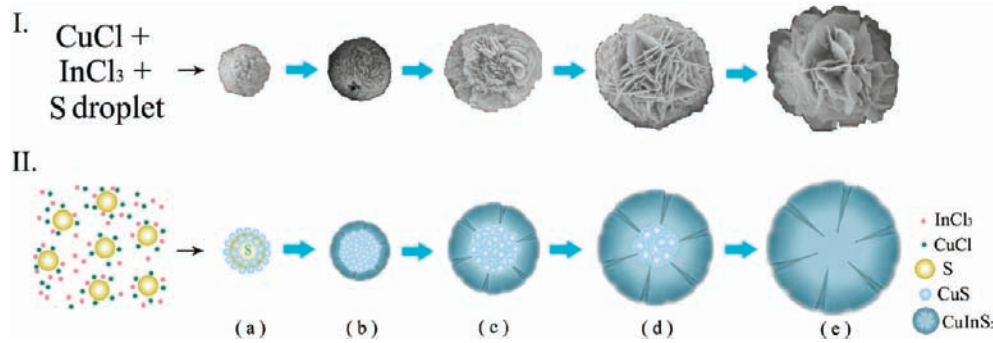

[a] (a) Melted sulfur droplets react with CuCl to form CuS nanoparticles on the surface. (b) CuS nanoparticles grow up to flakes and construct in situ formed CuS templates. (c) Small flakes aggregate together to large flakes, and CuS reacts with $InCl_3$ to form $CuInS_2$. (d) Continuous conversion from CuS to $CuInS_2$. (e) Pure $CuInS_2$ hierarchitectures.

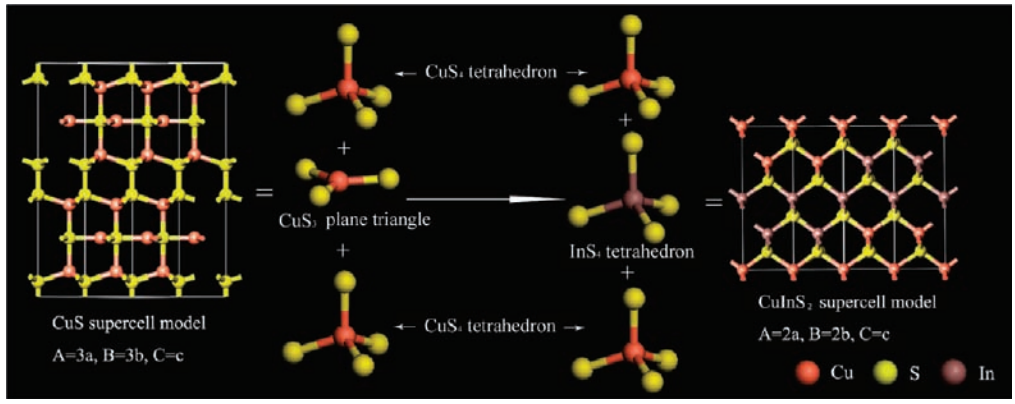

Figure 4. The atomic crystal structures and layer structures of CuS and $CuInS_2$ by supercell method.

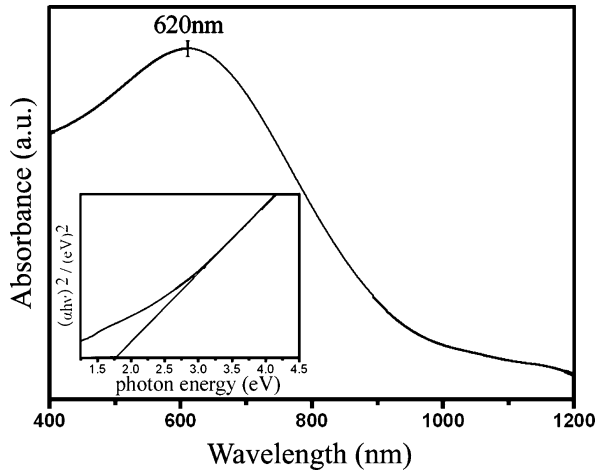

Figure 5. Typical UV−vis diffuse reflection spectrum of the $CuInS_2$ hierarchitectures and the bandgap value (the inset, estimated by a related curve of $(\alpha h\nu)^2$ versus photon energy plotted).

of Figure 5, from the intersection of the extrapolated linear portion. The value representing the band gap of the obtained $CuInS_2$ hierarchitectures can be determined as 1.80 eV, higher than the $CuInS_2$ photocatalyst reported in previous literature[14] and bulk $CuInS_2$ (1.53 eV). Combined with the fine monodispersity and hierarchically porous structure, the ability to absorb visible light makes the $CuInS_2$ microspheres an effective photocatalyst for solar-driven applications.

The as-obtained microcrystalline $CuInS_2$ hierarchitectures with good monodispersity and hierarchical structure of high surface area and surface permeability could provide sufficient visible-light response and ideal reaction sites for photocatalytic H_2 evolution. Figure 6 shows the photocatalytic activity for the H_2 evolution of 250 mg of 0.5 wt % Pt-loaded $CuInS_2$ microspheres as a photocatalyst under irradiation with visible light. The H_2 produced was evacuated every 3 h in successive runs. A considerable amount of H_2 was evolved, with an average rate of 59.4 μmol/h, and the highest rate can reach 84.0 μmol/h for 1.0 g of catalysts, as shown in Figure 6, which is much higher than the results reported in previous literature reports[14] (0.53 μmol/h for 1.0 g of catalysts). The total amount of generated H_2 was over 460 μmol, and the turnover number exceeded 1.0 after 40 h of irradiation with visible light, which indicates that the reaction proceeds photocatalytically. After four run tests in one continuous reaction, the amount of hydrogen produced decreased to 70% compared with the initial photocatalytic activity. But the activity of the photocatalyst could be recovered in the fifth cycle until some Na_2S and Na_2SO_3 was added into the aqueous solution. Hence, we deduced that the decrease of H_2 evolution in previous runs was possibly due to the consumption of sacrificial reagents during the photocatalytic reaction. When the light was turned off (dark test) and the reaction cell was evacuated, no H_2 was evolved until reirradiated by visible light. The higher photocatalytic activity of the obtained hierarchical $CuInS_2$ architectures may be contributed by the wider band gap, good monodispersity, and fine permeability, which could prevent catalysts from

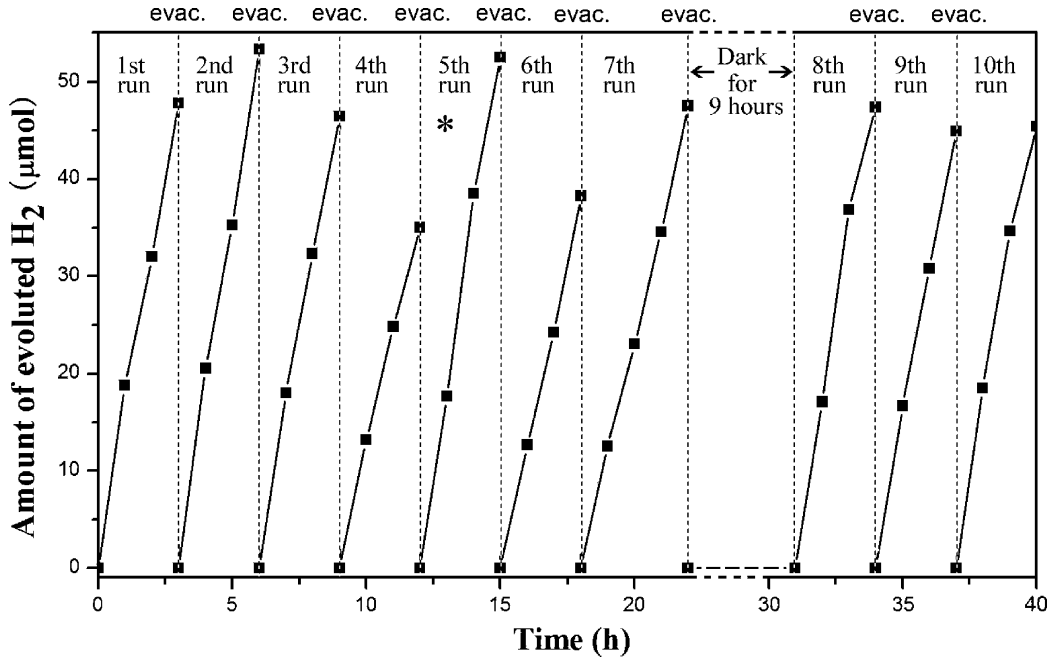

Figure 6. Time course of hydrogen yield over 0.250 g of Pt-loaded $CuInS_2$ hierarchitectures from an aqueous solution containing 0.35 M Na_2SO_3 and 0.25 M Na_2S under visible-light irradiation. *Adding Na_2SO_3 and Na_2S in 5th run due to the consumption of the sacrificial reagents.

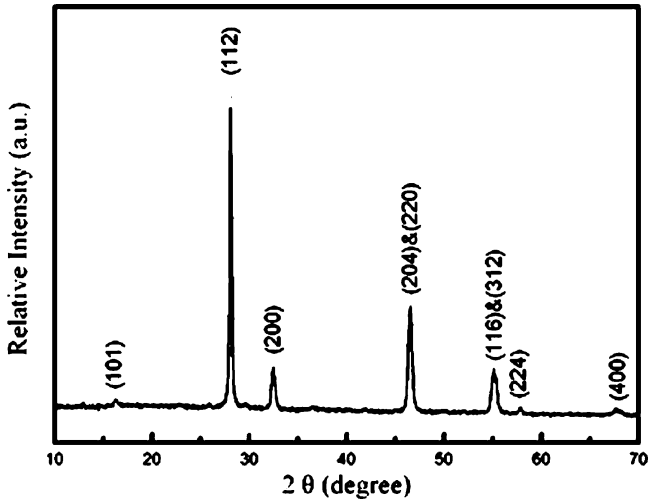

Figure 7. XRD pattern of the $CuInS_2$ product after the photocatalytic H_2 evolution.

having a large particle size and particle agglomeration. It has been verified that wider band gaps could compensate the effect of the overpotential for proton reduction to product H_2.[40] The low activity of bulk $CuInS_2$ to catalyze H_2 evolution from water even in the presence of sacrificial reagents indicates a large overpotential for H^+ reduction on the $CuInS_2$ surface. For $CuInS_2$ microarchitectures built with interleaving flakes, proton reduction is possible because the effect of the overpotential is compensated by the increased bandgap. Moreover, the catalysts were collected and dried after the catalytic reaction for further XRD characterization, and the XRD pattern is shown in Figure 7, in which one can clearly see that there were no significant changes in the XRD patterns of the catalyst before or after the reaction. Thus, we could be certain that the reaction for H_2 evolution under visible light irradiation is authentically catalytic.

(40) Frame, F.; Carroll, E.; Larsen, D.; Sarahan, M.; Browning, N.; Osterloh, F. *Chem. Commun.* **2008**, *19*, 2206.

4. Conclusions

In this work, we reported a new, one-pot solvothermal route for the large-scale preparation of nearly monodisperse $CuInS_2$ hierarchitectures using an in situ formed CuS template. On the basis of microscopic and structural observations, the intermediate CuS samples used as self-sacrificed templates play a critical role in the phase conversion and morphology retention for as-obtained $CuInS_2$ hierarchitectures. The present synthesis strategy simplified the previously reported methods for preparing ternary sulfides from binary sulfides via a two-step route and could be a general method for the ternary chalcogenide compounds with inherited and controlled shape and size. Significantly, the fabricated $CuInS_2$ sample with hierarchitecture and monodispersity exhibits a much enhanced visible-light-driven photocatalytic activity for H_2 evolution in successive runs compared to those reported in previous literature reports. In fact, the prepared materials are also believed to be exploited for applications in optoelectronic devices and solar energy conversion.

Acknowledgment. This work was financially supported by the National Natural Science Foundation of China (No.20621061) and the National Basic Research Program of China (No. 2009CB939901).

Supporting Information Available: SEM and TEM images and XRD patterns of CuS hierarchitectures obtained under various experimental conditions, and control experiment results from covellite CuS to chalcopyrite-type $CuInS_2$. This material is available free of charge via the Internet at http://pubs.acs.org.

IC802399F